The timing and cause of glacial activity during the last glacial in central Tibet based on ^{10}Be surface exposure dating east of Mount Jaggang, the Xainza range

Guocheng Dong [a, b, *], Weijian Zhou [a, b, c], Chaolu Yi [d, e], Yunchong Fu [a, b], Li Zhang [a, b], Ming Li [a, b]

[a] State Key Laboratory of Loess and Quaternary Geology, Institute of Earth Environment, Chinese Academy of Sciences, Xi'an 710061, China
[b] Xi'an AMS Center, Xi'an 710061, China
[c] Beijing Normal University, Beijing 100875, China
[d] Key Laboratory of Tibetan Environment Changes and Land Surface Process, Chinese Academy of Sciences, Beijing 100101, China
[e] Excellence Center for Tibetan Plateau Research, Chinese Academy of Sciences, Beijing 100101, China

ARTICLE INFO

ABSTRACT

Mountain glaciers are sensitive to climate change, and can provide valuable information for inferring former climates on the Tibetan Plateau (TP). The increasing glacial chronologies indicate that the timing of the local Last Glacial Maximum (LGM) recorded across the TP is asynchronous, implying different local influences of the mid-latitude westerlies and Asian Summer Monsoon in triggering glacier advances. However, the well-dated sites are still too few, especially in the transition zone between regions controlled by the two climate systems. Here we present detailed last glacial chronologies for the Mount Jaggang area, in the Xainza range, central Tibet, with forty-three apparent ^{10}Be exposure-ages ranging from 12.4 ± 0.8 ka to 61.9 ± 3.8 ka. These exposure-ages indicate that at least seven glacial episodes occurred during the last glacial cycle east of Mount Jaggang. These include: a local LGM that occurred at ~61.9 ± 3.8 ka, possibly corresponding to Marine Isotope Stage 4 (MIS 4); subsequent glacial advances at ~43.2 ± 2.6 ka and ~35.1 ± 2.1 ka during MIS 3; one glacial re-advance/standstill at MIS3/2 transition (~29.8 ± 1.8 ka); and three glacial re-advances/standstills that occurred following MIS 3 at ~27.9 ± 1.7 ka, ~21.8 ± 1.3 ka, and ~15.1 ± 0.9 ka. The timing of these glacial activities is roughly in agreement with North Atlantic millennial-scale climate oscillations (Heinrich events), suggesting the potential correlations between these abrupt climate changes and glacial fluctuations in the Mount Jaggang area. The successively reduced glacial extent might have resulted from an overall decrease in Asian Summer Monsoon intensity over this timeframe.

© 2018 Elsevier Ltd. All rights reserved.

1. Introduction

The behavior of mountain glaciers is a primary indicator of paleoclimate in high mountain ranges, where climate archives are relatively sparse, as compared with ocean basins or polar ice caps. Mountain glaciers react rapidly and markedly to changes in climate on sub-millennial timescales (Oerlemans, 2005), and thus glacial landforms, particularly moraines, have been widely dated to infer underlying climate changes in glaciated mountains (Balco, 2011),

such as those on the Tibetan Plateau (TP).

For the past two decades in particular, a large number of studies have been devoted to defining the timing and extent of glaciations throughout the TP, and to assessing possible mechanisms behind glacial fluctuations (e.g. Heyman, 2014 and references therein). These efforts parallel recent refinements in cosmogenic ^{10}Be surface exposure dating techniques. A large number of glacial chronologies on the TP (>2000 individual ^{10}Be exposure-ages) show that glaciers reached their maximum extent of the last glacial cycle (*ca.* 110–10 ka) prior to the global Last Glacial Maximum (LGM; *ca.* 26.5–19 ka; Clark et al., 2009) in many regions, suggesting high sensitivity of glaciers to variations in precipitation and thus to orbital-driven monsoon intensity (e.g. Phillips et al., 2000; Owen

et al., 2002a, 2002b; Finkel et al., 2003; Owen et al., 2003; Wang et al., 2013; Li et al., 2014; Chen et al., 2015). However, inter-regional and intra-regional differences have been observed that are likely influenced by the mid-latitude westerlies and Northern Hemisphere climate oscillations (e.g. Zech et al., 2013; Dong et al., 2014; Blomdin et al., 2016; Hu et al., 2016; Lehmkuhl et al., 2016). Regional differences in the timing of the local LGM are not necessarily surprising because mid-latitude mountain glaciers around the world are known to have reached their respective maximum extent at different times during the last glacial cycles (Gillespie and Molnar, 1995; Hughes et al., 2013). However, this does indicate that our understanding of the last glacial advances on the TP is incomplete and robust last glacial chronologies are sparse considering the vast TP. More data are needed to fully understand the forcing mechanisms behind glacial advances.

Tackling these problems requires a full understanding of glacial activities through time in the transition zone between the mid-latitude westerlies and Asian Summer Monsoon. Mount Jaggang is located in the middle of this zone, in central Tibet (Fig. 1A), and is influenced both by the westerlies and the Asian Summer Monsoon. Previous research has shown that the intensity of these two climate systems has varied in the past, on glacial-interglacial and glacial millennial timescales (An et al., 2012). Therefore our study offers an opportunity to better understand their relative influences through time in central Tibet. We examine glacial fluctuations during the last glacial cycle based on cosmogenic ^{10}Be surface exposure dating. We then compare the glacial chronologies with terrestrial, marine, and ice core records to identify climatic controls on glacial fluctuations during the last glacial in the Mount Jaggang area.

2. Study area

The Xainza range is located on the southern part of the central TP (Fig. 1A). This range is ~150 km in length and trends along a south-north direction. It rises from ~4900 m above sea level (asl) to the highest peak, Mount Jaggang, at 6444 m asl (Fig. 1B). The climate of this region is dominated by the southwest monsoon in summer and the mid-latitude westerlies in winter (Dong et al., 2010). At the Xainza weather station, ~13 km northeast of Mount Jaggang (Fig. 1B), the modern (1981–2012) mean annual temperature is 0.55 °C and the mean annual precipitation is 316 mm (Li et al., 2015).

Our study centers on the eastern slope of Mount Jaggang, where one glacial catchment consisting of two glacial valleys stretches ~3 km eastwards to the catchment mouth at an altitude of ~5370 m asl (Fig. 2A). Glaciers in the two valleys terminate at 5505 and 5605 m asl. Seven sets of moraines are distributed within ~2.0 km beyond the catchment mouth (Fig. 2). These moraines have been reworked by the glacial meltwater, which is feeding Gyaring Co Lake, ~19 km northwest of Mount Jaggang (Fig. 1B).

The outermost moraine (referred to as moraine JM1) forms a ~1.4 km-wide platform (Fig. 2). This moraine platform, ~70–140 m above the present river floor, extends downward to an altitude of ~4930 m asl where it forms a flat terminal-moraine crest. The surface of the moraine crest is mantled by a thin veneer of turf, on which boulders of >1 m in diameter are scattered. Some of these boulders contain cavernous pits up to 30 cm in diameter (Fig. 3H). Moraine JM1 is partially overlaid by a latero-frontal moraine (named moraine JM2) (Fig. 3A). Moraine JM2 is comprised of two latero-frontal crests, which can be traced upstream to the catchment mouth (Fig. 2). The crest of moraine JM2 rises ~130 m over that of moraine JM1. Those boulders embedded in the crest of moraine JM2 feature surficial knobs with diameters up to 20 cm (Fig. 3G). Inside of moraine JM2, another latero-frontal moraine (named moraine JM3) extends ~1 km eastward from the range-

front to an altitude of 5120 m asl. The distal part of moraine JM3 is characterized by a series of hummocks with a height of ~1–2 m (Fig. 3B and C). On the top of these hummocks, boulders protrude through sparse vegetation and reach 3 m in diameter.

A discontinuous inset moraine (named moraine JM4) can be distinguished along the proximal margin of moraine JM3 (Figs. 2 and 3B). In addition, three sets of moraine relics (referred to as moraine JM5, JM6, and JM7) are distributed between moraine JM4 and the dated Little Ice Age (LIA) moraine (Dong et al., 2017b) (Figs. 2A, C and 3D). The four moraines are characterized by crests with gentle relief of no more than 2 m, which commonly represent recessional moraines (Benn and Evans, 2010). The surface of these crests is sparsely vegetated, with emerging granitic boulders up to 3 m in diameter (Fig. 3D–F).

3. Methods

3.1. Mapping and sampling

Prior to the fieldwork, we identified the glacial features on the eastern slope of Mount Jaggang using oblique Google Earth imagery. These glacial features were then checked during field study in 2014–2016 to determine whether they might yield meaningful exposure-ages. After field investigations, we delineated the moraine sequences on the eastern slope of Mount Jaggang using a 30 m resolution ASTER GDEM (Global Digital Elevation Model; www.gscloud.cn) (Fig. 2A). Also, we illustrated these moraine sequences on the Google Earth images (Fig. 2B and C).

Forty-three glacial boulders were sampled from seven moraines (Moraine JM1-JM7) east of Mount Jaggang for ^{10}Be surface exposure dating. We preferentially selected the largest granitic boulders that were embedded in the moraine crest and characterized by rock varnish on the surface (Fig. 3F and supplementary material). Samples were collected from the top and flattest boulder surfaces using a hammer and chisel. The locations and elevations of all samples were recorded using a handheld GPS (global positioning system) instrument. The detailed geomorphic context was recorded through notes and photographs of sample locations (Supplementary material). Detailed sample information is provided in Table 1.

3.2. ^{10}Be surface exposure dating

Laboratory processing and ^{10}Be/^{9}Be ratio measurements were all performed at the Xi'an Accelerator Mass Spectrometry Center (Xi'an-AMS Center). After sample crushing and sieving (250–500 μm), quartz was isolated from the sample using the modified procedures of Kohl and Nishiizumi (1992), which were described in detail by Dortch et al. (2009) and Dong et al. (2014). The isolation of Be and precipitation of BeO were carried out following the procedure of Zhang et al. (2016). AMS measurements were made at the Xi'an-AMS Center based on the revised ICN standard (Nishiizumi et al., 2007, 07KNSTD). The measured ^{10}Be/^{9}Be ratios were corrected using four chemical procedural blanks (4.96×10^{-15}-20.13×10^{-15}) and converted to ^{10}Be concentrations for exposure-age calculation. Quartz weights, ^{9}Be carrier masses, measured ^{10}Be/^{9}Be ratios, and procedural blanks are shown in the Supplementary material.

Cosmogenic ^{10}Be exposure-ages were calculated using the CRONUS-Earth online calculator version 3 (Balco et al., 2008; http://hess.ess.washington.edu/), based on an assumption of zero erosion. In the interpretation, we focus on exposure-ages derived from the time- and nuclide-dependent scaling scheme LSDn (Lifton et al., 2014) on the basis of considerations as follows: Borchers et al. (2016) have demonstrated that the Lal (1991)/Stone (2000) time-
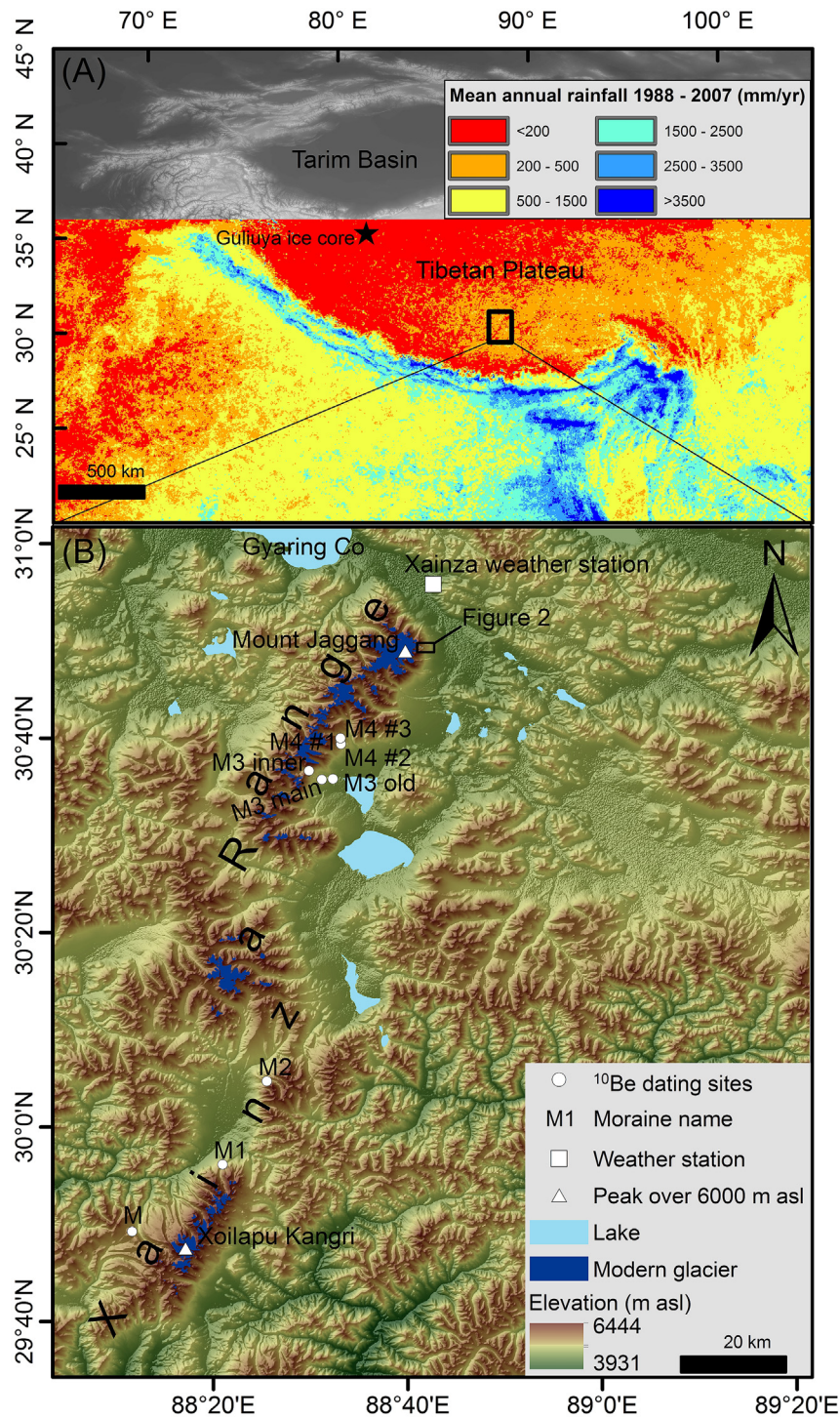
Fig. 1. Map showing location of the study area. (A) Shuttle radar topography mission (SRTM) digital elevation model (DEM) of the TP. Tropical Rainfall Measurement Mission (TRMM) average annual precipitation data for 1998–2008 (from Bookhagen and Burbank, 2006) is superimposed on the DEM. The black star shows the location of Guliya ice core. (B) A shaded relief map showing the specific location of the study area. White triangles show mountain peaks over 6000 m asl. White square indicates the location of the Xainza weather station. The black box shows the studied valley east of Mount Jaggang (Fig. 2). White dots illustrate the locations of moraines dated by Chevalier et al. (2011).

dependent and -independent scaling schemes have better fits to calibration datasets than those based on neutron monitors (e.g. Dunai, 2001; Desilets and Zreda, 2003; Lifton et al., 2005; Desilets et al., 2006); and the LSDn scaling scheme provides almost the same fits to datasets as the Lal (1991)/Stone (2000) scaling models but predicts scaling behavior more consistently at high-altitude and low-latitude locations (Lifton et al., 2014). We also reported

exposure-ages from scaling schemes based on neutron monitors (Supplementary material). Topographic shielding was determined using a python tool, developed by Li (2013), and the 30-m ASRTM DEM in the ArcGIS environment with designated 5° intervals in both azimuth and elevation angles. Rock density was assigned as 2.7 g/cm^3. No corrections were carried out for erosion, vegetation, or snow cover. Therefore, the ^{10}Be exposure-ages in this study are
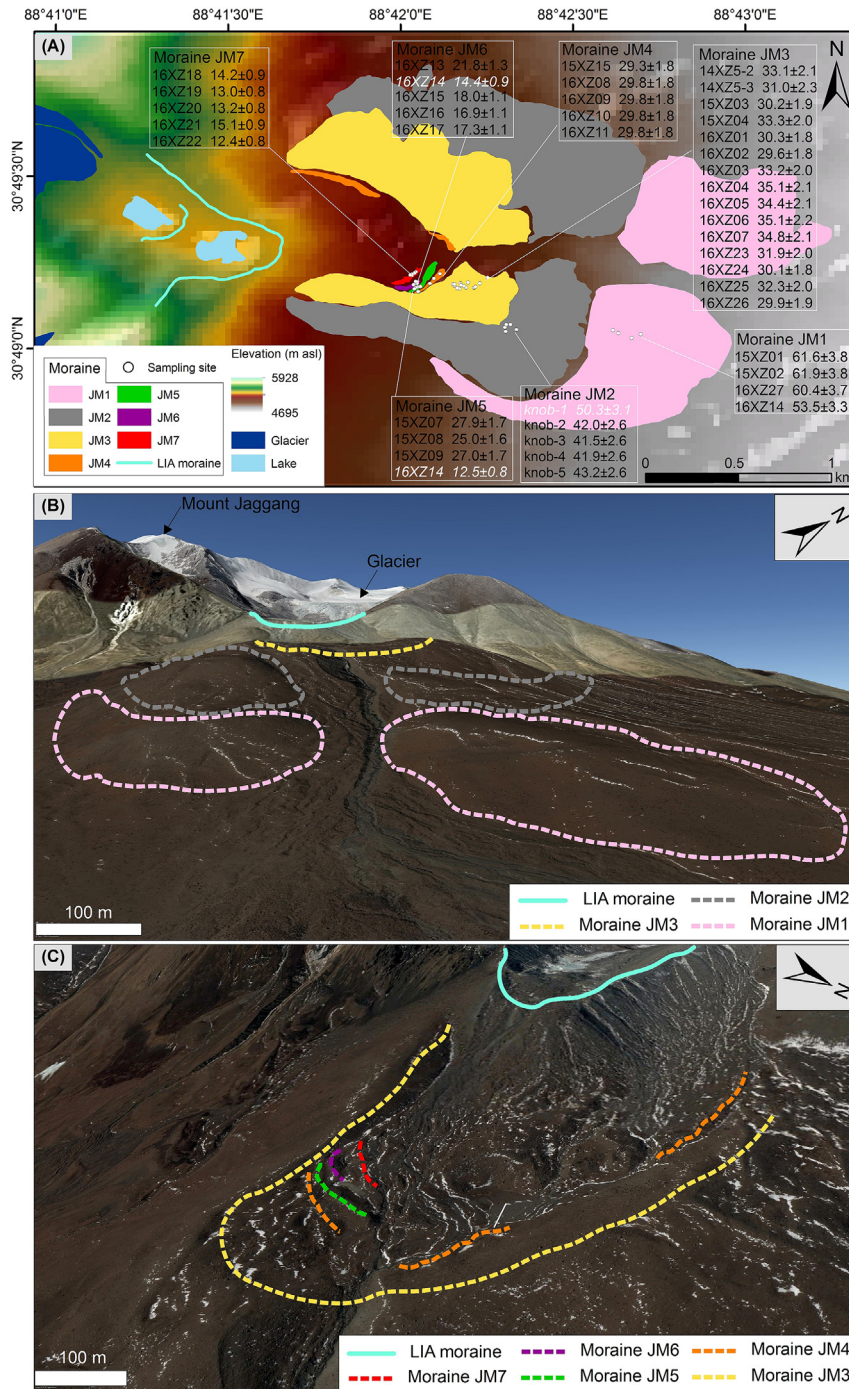
Fig. 2. (A) Detailed shaded relief map illustrating moraines east of Mount Jaggang. The Little Ice Age moraines are depicted following Dong et al. (2017b). The dating results are reported in the white box with one sigma external uncertainties. The potential outliers are shown with white text. (B) Oblique Google Earth image illustrating the LIA moraine and moraine JM 1, JM2, and JM3. (C) Oblique Google Earth image showing moraine JM3-JM7 and the LIA moraine.

considered as minimum ages.

3.3. Determination of moraine formation age

In ideal conditions, exposure-ages of boulders should represent the moraine formation age, while the spread in ages from a single moraine is often greater than would be expected from measurement uncertainties due to that boulders may have experienced prior exposure before their deposition or post-depositional reworking (Gosse and Phillips, 2001). Different strategies have

therefore been used to interpret scattered ages and to determine moraine depositional age (e.g. Balco, 2011 and references therein). In this study, to examine exposure-ages consistently, the potential outliers were statistically determined by identifying those exposure-ages which did not overlap within 1σ uncertainty with the others in a data set (e.g. Chevalier et al., 2011; Xu et al., 2013; Xu and Yi, 2014). Note that, as underlined by Chevalier et al. (2011), this strategy of outlier rejection is somewhat subjective, and thus we will discuss each moraine case by case. After removing the potential outlier(s), we use the maximum age of a moraine sample set to

Fig. 3. Selected photographs showing glacial landforms east of Mount Jaggang. (A) Looking eastwards from the distal part of moraine JM2. (B) Looking eastwards at the Little Ice Age moraine (Dong et al., 2017b). The white dashed lines show moraines JM3 and JM4. (C) Photographs showing the hummocky surface of moraine JM3. (D) Looking up-valley from moraine JM5. The white dashed lines illustrate the LIA moraine and moraine JM3, JM5, JM6, and JM7. (E) View of moraine JM4 and JM5 on moraine JM6. (F) Sample (16XZ20) that characterized by brown rock varnish on boulder surface. (G) Boulder featuring knob on the surface. (H) Boulder sampled from moraine JM1, which has a knob and cavernous pit on the surface. (For interpretation of the references to colour in this figure legend, the reader is referred to the Web version of this article.)

Table 1
Measured [10]Be concentrations and other parameters for boulders sampled from east of Mount Jaggang.

Moraine name	Sample ID	Latitude (°N)	Longitude (°E)	Elevation (m asl)	Boulder size, L/W/H (cm)	Sample thickness (cm)	Topographic shielding factor	[10]Be concentration (10[3] atoms g[−1])[a]
JM1	15XZ01	30.81755	88.71026	4942	95/73/64	4.2	0.9881	4666.2 ± 54.7
	15XZ02	30.81741	88.71053	4942	71/60/55	3.3	0.9932	4757.6 ± 55.4
	16XZ27	30.81718	88.71117	4932	263/196/86	5.3	0.9928	4512.9 ± 54.9
	16XZ28	30.81736	88.71161	4928	193/107/71	5.5	0.9928	4023.2 ± 63.6
JM2	Knob-1	30.81749	88.70508	5108	140/73/50 (19/12.5/5.5)	1.1	0.9912	4361.6 ± 68.4
	Knob-2	30.81769	88.70504	5106	210/108/80 (14.5/11/5)	1.5	0.9923	3764.0 ± 51.3
	Knob-3	30.81782	88.70511	5105	165/112/74 (8/6/6.5)	3.5	0.9923	3641.6 ± 56.5
	Knob-4	30.81758	88.70560	5094	260/170/75 (27/20/6)	5.9	0.9923	3593.8 ± 57.8
	Knob-5	30.81782	88.70531	5114	215/145/31 (17/8/5.5)	1.3	0.9923	3893.6 ± 49.8
JM3	14XZ5-2	30.8196	88.70355	5156	178/173/130	3.6	0.9923	2832.6 ± 61.2
	14XZ5-3	30.81961	88.70357	5155	71/55/43	5.3	0.9923	2654.7 ± 109.9
	15XZ03	30.82011	88.7042	5144	75/50/45	6.1	0.9920	2559.8 ± 42.5
	15XZ04	30.81965	88.70362	5155	253/178/167	6.2	0.9923	2778.9 ± 41.3
	16XZ01	30.81982	88.70383	5155	145/107/44 (16/10/5)	5.4	0.9915	2593.7 ± 32.0
	16XZ02	30.81956	88.70285	5155	225/120/60	5.7	0.9915	2518.5 ± 37.0
	16XZ03	30.81961	88.70316	5143	143/89/36	3.5	0.9923	2822.2 ± 35.6
	16XZ04	30.81986	88.70326	5155	284/137/111	5.0	0.9923	2985.0 ± 41.7
	16XZ05	30.81969	88.70306	5158	88/65/38	3.0	0.9923	2953.1 ± 46.2
	16XZ06	30.81982	88.70290	5152	232/142/73	4.0	0.9923	3009.9 ± 47.5
	16XZ07	30.81973	88.70292	5154	145/107/44	2.6	0.9923	3001.4 ± 43.1
	16XZ23	30.81970	88.70261	5154	677/620/133	5.3	0.9919	2709.7 ± 40.3
	16XZ24	30.81978	88.70254	5159	261/161/64	5.4	0.9919	2582.5 ± 38.8
	16XZ25	30.81977	88.70261	5156	113/103/33	5.4	0.9919	2735.8 ± 39.0
	16XZ26	30.81959	88.70274	5154	147/138/79	5.9	0.9919	2540.3 ± 55.4
JM4	15XZ10	30.82029	88.70190	5186	121/85/72	5.5	0.9904	2532.1 ± 39.5
	16XZ08	30.81981	88.70142	5183	139/61/51	4.5	0.9915	2597.3 ± 42.6
	16XZ09	30.82006	88.70161	5180	138/100/71	1.5	0.9915	2656.2 ± 46.0
	16XZ10	30.81942	88.70087	5183	223/149/81 (15/13/6)	4.5	0.9904	2599.6 ± 41.1
	16XZ11	30.81942	88.70085	5182	112/81/63	5.5	0.9904	2442.9 ± 40.8
JM5	15XZ07	30.81965	88.70083	5186	148/101/49	1.2	0.9904	2488.7 ± 35.4
	15XZ08	30.81961	88.70074	5186	175/90/68	7.5	0.9904	2092.9 ± 49.7
	15XZ09	30.81955	88.70067	5186	94/72/45	4.5	0.9904	2339.4 ± 47.6
	16XZ12	30.81966	88.70096	5185	118/87/83	2.5	0.9915	9156.9 ± 20.7
JM6	16XZ13	30.81975	88.70063	5187	81/68/32	2.5	0.9904	1850.9 ± 29.4
	16XZ14	30.81989	88.70081	5185	182/74/71	2.5	0.9904	1133.3 ± 27.1
	16XZ15	30.81980	88.70076	5185	303/266/103	1.1	0.9904	1481.3 ± 28.9
	16XZ16	30.81981	88.70080	5185	79/42/32	6.1	0.9904	1319.5 ± 26.3
	16XZ17	30.81991	88.70073	5185	100/85/40	2.5	0.9904	1401.3 ± 22.6
JM7	16XZ18	30.82038	88.70074	5187	234/188/100	1.1	0.9903	1137.8 ± 19.1
	16XZ19	30.82032	88.70067	5188	143/76/32	1.1	0.9903	1012.3 ± 23.1
	16XZ20	30.82021	88.70055	5188	102/64/42	0.9	0.9903	1028.4 ± 18.8
	16XZ21	30.82027	88.70055	5188	131/102/64	2.5	0.9903	1204.6 ± 24.9
	16XZ22	30.82023	88.70047	5186	112/75/66	3.5	0.9903	924.1 ± 19.7

[a] See Supplementary material for complete [10]Be data including sample and carrier weight and the measured sample and blank ratios.

4. Results and interpretation

Apparent [10]Be exposure-ages are listed in Table 2 and illustrated in Figs. 2A and 4. Forty-three exposure-ages from seven moraines range from 12.4 ± 0.8 ka to 61.9 ± 3.8 ka (Table 2) and generally conform well to their morphostratigraphical positions (Fig. 4).

Four samples collected from moraine JM1 yielded apparent exposure-ages ranging from 53.5 ± 3.3 ka to 61.9 ± 3.8 ka, which have a mean of 59.3 ± 4.0 ka (Fig. 4). No outliers can be statistically

closely represent the minimum moraine emplacement age, based on the consideration that exposure-ages from moraines are more likely to have a young bias due to post-glacial geomorphic progresses inducing incomplete exposure (e.g. Phillips et al., 1996; Putkonen and Swanson, 2003; Briner et al., 2005; Scherler et al., 2010; Heyman et al., 2011a, 2011b; Fu et al., 2013; Dong et al., 2014, 2017a). However, we acknowledge that these are still tentatively constrained moraine ages.

identified. Note that, however, the age of 53.5 ± 3.3 ka is slightly younger than the other three relatively clustered ages (Fig. 4). This implies that boulder 16XZ-28 may have experienced post-glacial shielding, confirming the field observation that the surface of this boulder appears to be more weathered compared with those of the other three boulders (Supplementary material). Assigning the oldest age 61.9 ± 3.8 ka as the formation age of moraine JM1 suggests a glacial advance during Marine Isotope Stage 4 (MIS 4) for the Mount Jaggang area.

Five knobs (knob1-5) protruding from the surface of boulders from moraine JM2 had apparent exposure-ages of 41.5 ± 2.6−50.3 ± 3.1 ka (Table 2), with a mean of 43.8 ± 3.7 ka (Fig. 4). If the oldest age 50.3 ± 3.1 ka, which seems different from the others at the 1σ level, is rejected as an outlier, the remaining four exposure-ages are generally consistent and have the oldest age of 43.2 ± 2.6 ka (Fig. 4), suggesting that moraine JM2 was possibly deposited during mid-MIS 3. We acknowledge that, from morphostratigraphic considerations, we cannot fully rule out a possibility

Table 2
Apparent [10]Be exposure-ages calculated using three scaling schemes.

Moraine name	Sample ID	St[a] (ka)			Lm[b] (ka)			LSDn[c] (ka)		
		Age	External uncertainty	Internal uncertainty	Age	External uncertainty	Internal uncertainty	Age	External uncertainty	Internal uncertainty
JM1	15XZ01	68.1	5.5	0.8	63.1	4.9	0.8	61.6	3.8	0.7
	15XZ02	68.6	5.6	0.8	63.5	4.9	0.8	61.9	3.8	0.7
	16XZ27	66.5	5.4	0.8	61.9	4.8	0.8	60.4	3.7	0.7
	16XZ28	59.3	4.9	1.0	55.7	4.3	0.9	53.5	3.3	0.9
JM2	Knob-1	57.3	4.7	0.9	53.5	4.2	0.9	50.3	3.1	0.8
	Knob-2	49.5	4.0	0.7	44.1	3.4	0.6	42.0	2.6	0.6
	Knob-3	48.7	4.0	0.8	43.4	3.4	0.7	41.5	2.6	0.7
	Knob-4	49.3	4.0	0.8	43.9	3.4	0.7	41.9	2.6	0.7
	Knob-5	51.0	4.1	0.7	45.4	3.5	0.6	43.2	2.6	0.6
JM3	14XZ5-2	37.0	3.1	0.8	34.3	2.7	0.7	33.1	2.1	0.7
	14XZ5-3	35.1	3.2	1.5	32.4	2.8	1.4	31.0	2.3	1.3
	15XZ03	34.3	2.8	0.6	31.5	2.4	0.5	30.2	1.9	0.5
	15XZ04	37.1	3.0	0.6	34.4	2.7	0.5	33.3	2.0	0.5
	16XZ01	34.4	2.8	0.4	31.6	2.4	0.4	30.3	1.8	0.4
	16XZ02	33.5	2.7	0.5	30.6	2.4	0.5	29.6	1.8	0.4
	16XZ03	37.0	3.0	0.5	34.3	2.6	0.4	33.2	2.0	0.4
	16XZ04	39.4	3.2	0.6	36.4	2.8	0.5	35.1	2.1	0.5
	16XZ05	38.3	3.1	0.6	35.4	2.7	0.6	34.4	2.1	0.5
	16XZ06	39.4	3.2	0.6	36.4	2.8	0.6	35.1	2.2	0.6
	16XZ07	38.9	3.2	0.6	35.9	2.8	0.5	34.8	2.1	0.5
	16XZ23	35.9	2.9	0.5	33.3	2.6	0.5	31.9	2.0	0.5
	16XZ24	34.2	2.8	0.5	31.4	2.4	0.5	30.1	1.8	0.5
	16XZ25	36.2	2.9	0.5	33.7	2.6	0.5	32.3	2.0	0.5
	16XZ26	33.8	2.8	0.7	31.0	2.4	0.7	29.9	1.9	0.7
JM4	15XZ10	33.2	2.7	0.5	30.4	2.3	0.5	29.3	1.8	0.5
	16XZ08	33.7	2.7	0.6	30.9	2.4	0.5	29.8	1.8	0.5
	16XZ09	33.7	2.7	0.6	30.9	2.4	0.5	29.8	1.8	0.5
	16XZ10	33.8	2.7	0.5	31.0	2.4	0.5	29.8	1.8	0.5
	16XZ11	32.0	2.6	0.5	29.4	2.3	0.5	28.4	1.8	0.5
JM5	15XZ07	31.4	2.5	0.5	28.9	2.2	0.4	27.9	1.7	0.4
	15XZ08	27.8	2.3	0.7	25.9	2.0	0.6	25.0	1.6	0.6
	15XZ09	30.4	2.5	0.6	28.0	2.2	0.6	27.0	1.7	0.6
	16XZ12	11.6	1.0	0.3	12.3	1.0	0.3	12.5	0.8	0.3
JM6	16XZ13	23.6	1.9	0.4	22.3	1.7	0.4	21.8	1.3	0.3
	16XZ14	14.4	1.2	0.3	14.6	1.2	0.4	14.4	0.9	0.3
	16XZ15	18.6	1.5	0.4	18.4	1.4	0.4	18.0	1.1	0.4
	16XZ16	17.3	1.4	0.3	17.2	1.3	0.3	16.9	1.1	0.3
	16XZ17	17.8	1.4	0.3	17.7	1.4	0.3	17.3	1.1	0.3
JM7	16XZ18	14.3	1.2	0.2	14.5	1.1	0.2	14.2	0.9	0.2
	16XZ19	12.7	1.0	0.3	13.2	1.0	0.3	13.0	0.8	0.3
	16XZ20	12.9	1.0	0.2	13.3	1.0	0.2	13.2	0.8	0.2
	16XZ21	15.3	1.3	0.3	15.4	1.2	0.3	15.1	0.9	0.3
	16XZ22	11.8	1.0	0.3	12.5	1.0	0.3	12.4	0.8	0.3

Notes: [10]Be exposure-ages were calculated by using the CRONUS earth calculator version 3 (Balco et al., 2008) with an assumption of absence of surface erosion and rock density of 2.7 g/cm^{3}.

[a] St represents constant production rate model of Lal (1991)/Stone (2000).
[b] Lm represents time-varying production meodl of Lal (1991)/Stone (2000).
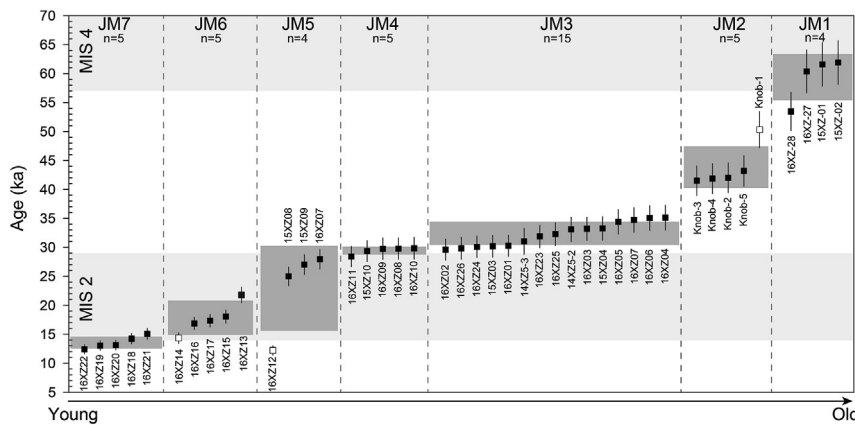[c] LSDn represents time- and nuclide-dependent scaling model (Lifton et al., 2014).

Fig. 4. [10]Be exposure-ages plotted by relative moraine ages for the Mount Jaggang area. Exposure-ages are illustrated by rectangles, next to which the sample ID is listed. The number of samples is shown for each moraine, as well as the potential outliers (in white). The dark grey-shaded boxes represent the mean age for each moraine (including the potential outliers). The two light grey-shaded boxes illustrate the cold periods corresponding to MIS 4 and 2.

that moraine JM2 may have correlated with an early MIS 3 glacial advance around 50.3 ± 3.1 ka. However, it is more rigorous to tentatively attribute moraine JM2 to mid-MIS 3 glacial advance because four roughly clustered ages fall well into this period.

Boulders sampled from moraine JM3 produced fifteen apparent exposures-ages ranging from 29.6 ± 1.8 ka to 35.1 ± 2.1 ka (Table 2), which all spanned the late MIS 3 interval. The spread of ages appears regular and no outliers can be identified (Fig. 4). It is interesting to note that the distal part of moraine JM3 is characterized by hummocks (Fig. 3B and C), suggesting a lengthy period of landform surface instability (Çiner et al., 2015) that contributes to the potential of moraine degradation and boulder destabilization. In such a scenario, the oldest age may provide the best estimate of moraine depositional age (Zech et al., 2005b; Crump et al., 2017). This further convinces us to use the oldest age (35.1 ± 2.1 ka) to constrain the initial moraine age. This suggests that moraine JM3 record a late MIS 3 glacial advance.

Five highly clustered exposure-ages were obtained from the inset moraine JM4. These exposure-ages had a range of $28.4 \pm 1.8 - 29.8 \pm 1.8$ ka and a mean of 29.4 ± 0.6 ka (Table 2; Fig. 4). Using the oldest one to define the moraine formation age implies a glacial re-advance/standstill that corresponds to late MIS 3 or early MIS 2.

Four samples collected from the recessional moraine JM5 had exposure-ages of $12.2 \pm 0.8 - 27.9 \pm 1.7$ ka (Table 2) that have a mean age of 23.0 ± 7.3 ka (Fig. 4). The age of 12.2 ± 0.8 is obviously younger than the other three and is not overlapping with them at the 1σ level (Fig. 4), implying that post-depositional processes (for example, boulder exhumation and rotation) may have played an important role in sample 16XZ12. Removing this sample results in a roughly clustered small subset (Fig. 4). The oldest one of this subset constrains the age of moraine deposition to 27.9 ± 1.7 ka, reflecting an early MIS 2 glacial event.

Five apparent exposure-ages from the recessional moraine JM6 ranged from 14.4 ± 0.9 ka to 21.8 ± 1.3 ka (Table 2). At the 1σ level, the maximum and minimum ages do not overlap with the remaining three ages (Fig. 4). The youngest age of 14.4 ± 0.9 ka is likely caused by post-glacial geomorphic processes, such as weathering, boulder exhumation, and toppling, which have been widely reported in previous work (e.g. Hallet and Putkonen, 1994; Putkonen and Swanson, 2003; Heyman et al., 2011b, 2016). Although the oldest age, 21.8 ± 1.3 ka, appears to reflect a boulder containing low-level inheritance, however, we hesitate to reject this age as an outlier because this age as well as the next oldest age are within the global LGM chronozone levels (19–23 cal ka or 18–24 cal ka) defined by Mix et al. (2001). This implies that moraine JM6 likely marked the global LGM glacial fluctuation.

The adjacent recessional moraine, JM7, provided five exposure-ages having a range of $12.4 \pm 0.8 - 15.1 \pm 0.9$ ka and a mean of 13.6 ± 1.6 ka (Table 2). No outlier is identified from this moraine (Fig. 4). If we use the oldest age 15.1 ± 0.9 to represent the moraine formation age, moraine JM7 document a last deglacial event that possibly correspond to Heinrich Stadial 1 (HS1; Hemming, 2004).

5. Discussion

5.1. The last glacial chronologies east of Mount Jaggang

Forty-three apparent [10]Be exposure-ages from seven moraines east of Mount Jaggang suggest that three glacial advances and two re-advances/standstills occurred prior to the global LGM, and that two following glacial re-advances/standstills possibly occurred in the global LGM and the last deglacial, respectively. Also, we re-evaluated 54 [10]Be exposure-ages from nine moraines across the Xainza range (Chevalier et al., 2011, Fig. 1B), most of which fell within the last glacial periods (Table 3). In order to compare our results with these data, we recalculated all of the ages using the CRONUS-Earth online calculator version 3 with the time- and nuclide-dependent scaling scheme LSDn (Lifton et al., 2014) (Table 3). We used the sample density, sample thickness, and other parameters furnished by Chevalier et al. (2011). We rejected outliers following the original publication: ages twice as old as the next oldest age were firstly excluded as outliers with inheritance; additional potential outliers were identified by examining ages whose uncertainty (1σ) did not overlap with the others (Chevalier et al., 2011). The exposure-ages from moraine M3-old (Fig. 1B) predate the last glacial periods (Chevalier et al., 2011, Table 3) and are beyond the scope of this study, so we have not discussed these ages.

5.1.1. Late MIS 5 (ca. 110–71 ka)

No glacial evidence has been identified during late MIS 5 east of Mount Jaggang. Only occasional boulders from individual moraines (moraine M4 #3b and M4 #3c) (Chevalier et al., 2011, Table 3), ~20 km southwest of Mount Jaggang (Fig. 1B), were found to correspond to late MIS 5 (Table 3). It is important to note, however, that the number of exposure-age is too small to determine the moraine depositional age. So at present, the question of whether the glacier advanced during MIS 5 across the Xainza range remains equivocal. This is also an open question for other regions of the TP and its surroundings (Owen and Dortch, 2014) despite suggestions that MIS 5 glacial advances occurred in some semi-arid regions of the TP (e.g. Amidon et al., 2013; Dortch et al., 2013; Zech, 2012; Zech et al., 2013; Blomdin et al., 2016; Rother et al., 2017; Yang et al., 2017).

5.1.2. MIS 4 (ca. 71–57 ka)

There is evidence for glacial fluctuations during MIS 4 from our dataset. The moraine platform (JM1) east of Mount Jaggang recorded a glacial advance around 61.9 ± 3.8 ka, signifying that the local LGM likely occurred during MIS 4 in the Mount Jaggang area. The recalculated exposure-ages from moraine M4 #3a (Fig. 1B) also gave a maximum age of 62.1 ± 3.8 ka (Table 3) that was in accord with MIS4, after excluding two seemingly old outliers as suggested by Chevalier et al. (2011). However, the recalculated five exposure-ages on moraine M4 #3a are highly scattered and not overlapping with each other (Table 3). Therefore, it is not unambiguous whether moraine M4 #3a was formed during MIS4. MIS 4 glaciation has been proposed as the local LGM mainly in the westerly-influenced TP except the Himalayas (Owen et al., 2010), including the Tian Shan (Koppes et al., 2008; Zhao et al., 2010; Zech, 2012; Li et al., 2014; Chen et al., 2015) and the Pamir Mountains (Zech et al., 2005a, 2013; Abramowski et al., 2006; Owen et al., 2012).

5.1.3. MIS 3 (ca. 57–29 ka)

Our results present a great number of apparent exposure-ages spanning the MIS 3 interval: four out of five samples on moraine JM2 had relatively concurrent ages (41.5–43.2 ka); fifteen apparent exposure-ages from a hummocky moraine (JM3) had an age range of 29.6–35.1 ka; and the inset moraine (JM4) yielded five highly consistent exposure-ages (Fig. 4 and Table 2). These exposure-ages indicate that glaciers advanced two or three times during MIS 3 east of Mount Jaggang. In addition, twenty-two apparent exposure-ages (without outliers) from moraine M1, M2, and M3 main (Fig. 1B) were re-calculated to $25.1 \pm 1.5 - 32.9 \pm 2.1$ ka, $29.3 \pm 1.8 - 50.3 \pm 3.0$ ka, and $36.3 \pm 2.2 - 41.1 \pm 2.5$ ka (Chevalier et al., 2011, Table 3), with most of which lying well within the MIS 3 timespan. If we use the maximum age in one age-group to represent the moraine formation age, moraine M2, M1 and, M3 main seemingly correspond to early-, late- and mid- MIS 3. While these assignments are tentative,

Table 3
Recalculated apparent [10]Be exposure-ages (Chevalier et al., 2011) from moraines in the other valleys of the Xainza range.

Moraine name	Sample ID[a]	St[b] Age	External uncertainty	Internal uncertainty	Lm[c] Age	External uncertainty	Internal uncertainty	LSDn[d] Age	External uncertainty	Internal uncertainty
M4 #3a	T7C-7	69.4	5.6	0.8	64.1	4.9	0.8	62.1	3.8	0.7
	T7C-11	*150.8*	*12.4*	*1.2*	*130.4*	*10.2*	*1.0*	*122.5*	*7.5*	*1.0*
	T7C-15	57.4	4.7	0.7	53.6	4.1	0.7	50.5	3.1	0.6
	T7C-17	*102.4*	*8.4*	*1.3*	*93.1*	*7.2*	*1.2*	*90.5*	*5.6*	*1.1*
	T7C-18	46.3	3.8	0.6	41.4	3.2	0.6	40.3	2.5	0.6
M4 #3b	T7C-14	132.3	10.9	1.2	115.9	9.0	1.1	110.3	6.8	1.0
M4 #3c	T7C-12	88.7	7.2	0.8	81.4	6.3	0.7	78.0	4.7	0.7
M3-old	T7C-19	295.2	25.5	4.0	248.5	20.1	3.4	234.5	15.0	3.2
	T7C-20	471.4	42.3	5.1	394.2	32.9	4.2	372.7	24.5	4.0
	T7C-21	422.3	37.4	4.2	350.4	28.9	3.4	327.7	21.3	3.2
	T7C-22	*742.8*	*71.3*	*6.2*	*610.9*	*53.8*	*4.9*	*577.6*	*39.8*	*4.6*
	T7C-23	216.1	18.2	2.4	185.8	14.7	2.0	179.2	11.2	2.0
M3 main	*T7C-24*	*61.8*	*5.0*	*0.9*	*58.0*	*4.5*	*0.9*	*56.1*	*3.5*	*0.8*
	T7C-24bis	*65.2*	*5.4*	*1.2*	*60.9*	*4.8*	*1.1*	*59.2*	*3.7*	*1.1*
	T7C-25	44.2	3.6	0.7	40.1	3.1	0.6	39.2	2.4	0.6
	T7C-26	44.7	3.6	0.5	40.4	3.1	0.5	39.5	2.4	0.5
	T7C-27	47.9	3.9	0.7	42.7	3.3	0.6	41.1	2.5	0.6
	T7C-28	40.6	3.3	0.6	37.3	2.9	0.5	36.3	2.2	0.5
	T7C-30	46.8	3.8	0.5	41.8	3.2	0.5	40.6	2.5	0.5
M3 inner	T7C-32	17.1	1.4	0.2	17.0	1.3	0.2	16.6	1.0	0.2
	T7C-33	12.2	1.0	0.3	12.8	1.0	0.3	12.8	0.8	0.3
	T7C-34	12.4	1.0	0.2	13.0	1.0	0.2	12.9	0.8	0.2
	T7C-35	14.0	1.1	0.2	14.3	1.1	0.2	14.0	0.9	0.2
	T7C-36	12.9	1.1	0.3	13.3	1.0	0.3	13.1	0.8	0.3
	T7C-37	13.5	1.1	0.3	13.9	1.1	0.3	13.7	0.9	0.3
	T7C-39	14.7	1.2	0.3	14.9	1.2	0.3	14.6	0.9	0.3
M2	T7C-40	52.8	4.3	0.6	47.5	3.6	0.5	44.6	2.7	0.5
	T7C-41	47.4	3.8	0.6	42.1	3.2	0.5	40.8	2.5	0.5
	T7C-42	36.2	2.9	0.4	33.5	2.6	0.4	32.2	2.0	0.4
	T7C-43	*16.3*	*1.3*	*0.2*	*16.4*	*1.3*	*0.2*	*16.1*	*1.0*	*0.2*
	T7C-44	45.6	3.7	0.8	40.9	3.2	0.7	39.9	2.5	0.7
	T7C-45	*23.4*	*1.9*	*0.3*	*22.1*	*1.7*	*0.3*	*21.7*	*1.3*	*0.3*
	T7C-46	57.4	4.6	0.6	53.6	4.1	0.5	50.3	3.0	0.5
	T7C-47	38.5	3.1	0.4	35.4	2.7	0.4	34.5	2.1	0.3
	T7C-49	*16.6*	*1.3*	*0.2*	*16.5*	*1.3*	*0.2*	*16.3*	*0.2*	*1.0*
	T7C-50	37.7	3.0	0.5	34.8	2.7	0.4	34.0	2.1	0.4
	T7C-51	33.0	2.7	0.5	30.1	2.3	0.4	29.3	1.8	0.4
M1	T7C-63	29.4	2.4	0.4	27.1	2.1	0.3	26.3	1.6	0.3
	T7C-64	27.8	2.2	0.4	25.7	2.0	0.3	25.1	1.5	0.3
	T7C-65	31.3	2.5	0.4	28.7	2.2	0.4	28.0	1.7	0.4
	T7C-66	30.2	2.5	0.7	27.8	2.2	0.7	27.1	1.7	0.6
	T7C-68	32.2	2.6	0.4	29.5	2.3	0.4	28.7	1.7	0.4
	T7C-69	32.3	2.7	0.9	29.6	2.4	0.8	28.8	1.9	0.8
	T7C-70	27.7	2.2	0.3	25.6	2.0	0.3	25.0	1.5	0.3
	T7C-71	32.2	2.7	0.8	29.5	2.4	0.8	28.7	1.9	0.7
	T7C-72	36.5	3.0	0.7	33.8	2.6	0.7	32.9	2.1	0.7
M	T7C-55	12.9	1.0	0.2	13.4	1.0	0.2	13.2	0.8	0.2
	T7C-56	*28.0*	*2.3*	*0.5*	*26.0*	*2.0*	*0.5*	*25.2*	*1.6*	*0.5*
	T7C-57	17.2	1.4	0.3	17.1	1.3	0.3	16.8	1.0	0.3
	T7C-58	16.0	1.3	0.4	16.0	1.3	0.4	15.7	1.0	0.4
	T7C-59	*36.0*	*2.9*	*0.4*	*33.3*	*2.5*	*0.4*	*32.0*	*1.9*	*0.4*
	T7C-60	15.8	1.3	0.5	15.9	1.3	0.5	15.6	1.0	0.5
	T7C-61	21.0	1.7	0.3	20.4	1.6	0.3	20.1	1.2	0.3
	T7C-62	*78.0*	*6.3*	*0.9*	*71.3*	*5.5*	*0.8*	*68.1*	*4.2*	*0.8*

[a] The bold italic indicates samples that were considered as potential outliers by Chevalier et al. (2011).
[b] St represents constant production rate model of Lal (1991)/Stone (2000).
[c] Lm represents time-varying production meodl of Lal (1991)/Stone (2000).
[d] LSDn represents time- and nuclide-dependent scaling model (Lifton et al., 2014).

it is clear that glaciers advanced during MIS 3 in the Xainza range as reported elsewhere across the TP, such as the Himalayas (Phillips et al., 2000; Owen et al., 2002a, 2010; Finkel et al., 2003; Dortch et al., 2013), the Karakoram and Pamir Mountains (Owen et al., 2002b; Zech et al., 2005a; Abramowski et al., 2006; Seong et al., 2009; Röhringer et al., 2012), Anyemaqen and Nianbaoyeze Mountains (Owen et al., 2003), Mawang Kangri (Amidon et al., 2013), Nyainqentanglha (Dong et al., 2014), Dalijia Shan (Wang et al., 2013), and Tianshan (Koppes et al., 2008; Li et al., 2014; Chen et al., 2015).

5.1.4. MIS 2 (ca. 29–14 ka)

There were clear glacial fluctuations during MIS 2, with relatively clustered ages marking an early MIS 2 advance at ~27.9 ± 1.7 ka, the global LGM re-advance/standstill at ~21.8 ± 1.3 ka, and a post-LGM, possible HS1, re-advance/standstill around 15.1 ± 0.9 ka. Also, the recalculated exposure-ages indicate at least two glacial advances during this period: six out of eight exposure-ages from moraine M yield ages of 13.2 ± 0.8–25.2 ± 1.6 ka; and seven exposure-ages from moraine M3 inner range from 12.8 ± 0.8 to 16.6 ± 1.0 ka (Chevalier et al., 2011, Table 3). Moraine M and M3

inner appear to record glacial advances in the global LGM and last deglaciation, respectively. While ages from MIS 2 moraines are slightly scattered, we can say that the extent of the glaciers was restricted during the global LGM in the Xainza range, as suggested for the greater TP (e.g. Owen and Dortch, 2014). Glacial advance during HS 1 has been found only at limited sites on the TP, such as Basongcuo, the eastern Himalaya (Hu et al., 2016), the Zheduo Valley, southeastern TP (Strasky et al., 2009), and Muztag Ata and Kongur Shan, western TP (Seong et al., 2009).

5.1.5. The late glacial (ca. 14—10 ka)

There is no direct evidence of the late glacial fluctuations east of Mount Jaggang, despite that some of the dating results (Fig. 4 and Table 1) as well as the recalculated exposure-ages (Chevalier et al., 2011, Table 3) are coeval with this period. At present, we thus cannot elucidate the pattern of late glacial fluctuations across the Xainza range.

In summary, the dated moraines east of Mount Jaggang have preserved evidence of at least seven glacial events. The local LGM predates the global LGM, and appears to be in line with MIS 4. Two subsequent glacial advances occurred in mid- and late-MIS 3. An inset moraine (moraine JM4) documents a re-advance/standstill during the MIS 3/2 transition. Three recessional moraines (moraine JM5, JM6, and JM7) mark re-advances or standstills during early MIS 2, the global LGM, and the last deglaciation. The last deglacial fluctuation is generally in agreement with HS 1.

5.2. The cause of glacial advances

Glacial fluctuations are mainly controlled by variations in temperature and precipitation (Rupper et al., 2009). Determining the dominant forcing factors is complex, as they can vary temporally and regionally (Benn and Owen, 1998). The last glacial climatic changes have been documented by a combination of climatic proxies. These include summer insolation (Berger and Loutre, 1991), ice core $\delta^{18}O$ records (Thompson et al., 1997), a benthic $\delta^{18}O$ record (Lisiecki and Raymo, 2005), and a stalagmite $\delta^{18}O$ record (Wang et al., 2001) (Fig. 5). We consider below, possible forcing factors that influence glacial movements in the Mount Jaggang area during the last glacial.

The local LGM in the Mount Jaggang area occurred during MIS 4. The subsequent glacial advances became progressively less extensive through time, out-of-phase with the Northern Hemisphere ice sheet. Both the local and global LGM are in good agreement with low Northern Hemisphere summer insolation (Berger and Loutre, 1991, Fig. 5C) and periods of global ice expansion (Lisiecki and Raymo, 2005, Fig. 5B). The more restricted glacier extent over the TP during the global LGM has been attributed to relatively arid conditions, as compared with the early last glacial (e.g. Shi et al., 1997, 2001; Xu et al., 2013, 2014; Dong et al., 2017a). Arid conditions during the global LGM in the Mount Jaggang area could result from a weakened Asian Summer Monsoon (Wang et al., 2001, Fig. 5A). However, glacier extent in MIS 3, a relatively humid and warm period, was smaller than MIS 4, although more extensive than MIS 2 in the east of Mount Jaggang. Northern Hemisphere summer insolation during MIS 4 was lower than during MIS 2 or MIS 3 (Berger and Loutre, 1991, Fig. 5C), favoring a colder climate and glaciation.

Evidence for a MIS 3 glacial advance has been found in many places on the TP and its surrounding mountains (e.g. Phillips et al., 2000; Wang et al., 2013; Dong et al., 2014; Li et al., 2014; Chen et al., 2015). The Guliya ice core in the West Kunlun (Fig. 1) shows a relatively cold sub stage in mid-MIS 3 (Thompson et al., 1997, Fig. 5D), mirroring the relatively low local and high latitude summer insolation during this period (Berger and Loutre, 1991, Fig. 5C).

Most previous studies have highlighted the relatively cold climate as well as increased precipitation during mid-MIS 3 as triggers for glacial advance (e.g. Owen et al., 2002a; Shi and Yao, 2002; Wang, 2010). However, the constrained ages of these TP glacier advances extend beyond mid-MIS 3 (Wang, 2010). On a global scale, MIS 3 is a period with abrupt climate transitions between cold stadial, and mild interstadial, climate conditions (Voelker and workshop participants, 2002). Dong et al. (2014) have thus hypothesized multiple MIS 3 glacial advances for the western Nyainqentanglha Mountains, ~150 km southeast of Mount Jaggang, and proposed a link between these advances and Heinrich Stadials, recorded by Heinrich layers in the North Atlantic (Heinrich, 1988; Bond et al., 1993) and characterized by cooling. Some of these cooling events have been shown to exert a strong influence on the central TP (e.g. Kasper et al., 2015; Zhu et al., 2015; He et al., 2016). However, it still has to be resolved whether and how these cooling events at high-latitude are registered by glaciers on the central TP.

In the case of Mount Jaggang, moraines do document two MIS 3 glacial advances at ~43.2 ± 2.6 ka and ~35.1 ± 2.1 ka, which are approximately coeval with HS 5 and 4 (Fig. 5E), respectively. There is more evidence for the potential correlation between Heinrich events and glacial fluctuations in the Mount Jaggang area: the local LGM at ~61.9 ± 3.8 ka roughly corresponds to HS 6; a glacial re-advance/standstill around the MIS 3/2 transition, at ~29.8 ± 1.8 ka, is highly consistent with HS 3; and post-MIS 3 glacial re-advances/standstills occurred at ~27.9 ± 1.7 ka, ~21.8 ± 1.3 ka, and ~15.1 ± 0.9 ka, slightly later than HS 3, HS 2, and HS 1, respectively. Based on ^{10}Be surface exposure dating, Strasky et al. (2009) and Hu et al. (2016) also demonstrated the likelihood that glaciers advanced in the southeastern TP responded to HS 1 cooling following the global LGM. These correlations, although tentative, support a potential teleconnection between the North Atlantic Ocean and the TP. A great many studies have argued that the mid-latitude westerlies play a critical role in bringing cold air masses to the TP, hence connecting this region to the North Atlantic Ocean (e.g. Porter and An, 1995; Hong et al., 2003; Vandenberghe et al., 2006; Han et al., 2008; An et al., 2012).

Climatic changes over the central TP are currently dominated by variations in both the Asian Summer Monsoon and the mid-latitude westerlies (Dong et al., 2010). Hence, hemispheric cold events could promote glacial advances in the Mount Jaggang area during the last glacial. The mid-latitude westerlies are anti-correlated with the Asian Summer Monsoon on glacial-interglacial and glacial millennial timescales (An et al., 2012; Zhu et al., 2015). The intensity of the Asian Summer Monsoon decreased from the MIS 4/3 transition to the late glacial according to speleothem records from Hulu cave (Wang et al., 2001, Fig. 5A). Such aridification has also been revealed by a review of effective moisture reconstructions over the whole TP (Herzschuh, 2006). The declining intensity of the Asian Summer Monsoon during this period might have resulted in decreased precipitation in the Mount Jaggang area, and the stepwise shrinkage of glaciers.

Overall, activities of the last glacial glacier in the Mount Jaggang area, central Tibet, roughly occur at the same frequency as several of the North Atlantic Heinrich events. We thus infer that there was a close association between glacial activities east of Mount Jaggang and ice-rafting pulses in the North Atlantic Ocean. The cooling signals in the North Atlantic regions might have affected glacier advances/standstills east of Mount Jaggang via the mid-latitude westerlies.

5.3. Uncertainties in climate correlations

While we have tried to define the timing of glacial fluctuations east of Mount Jaggang and correlate these fluctuations with the
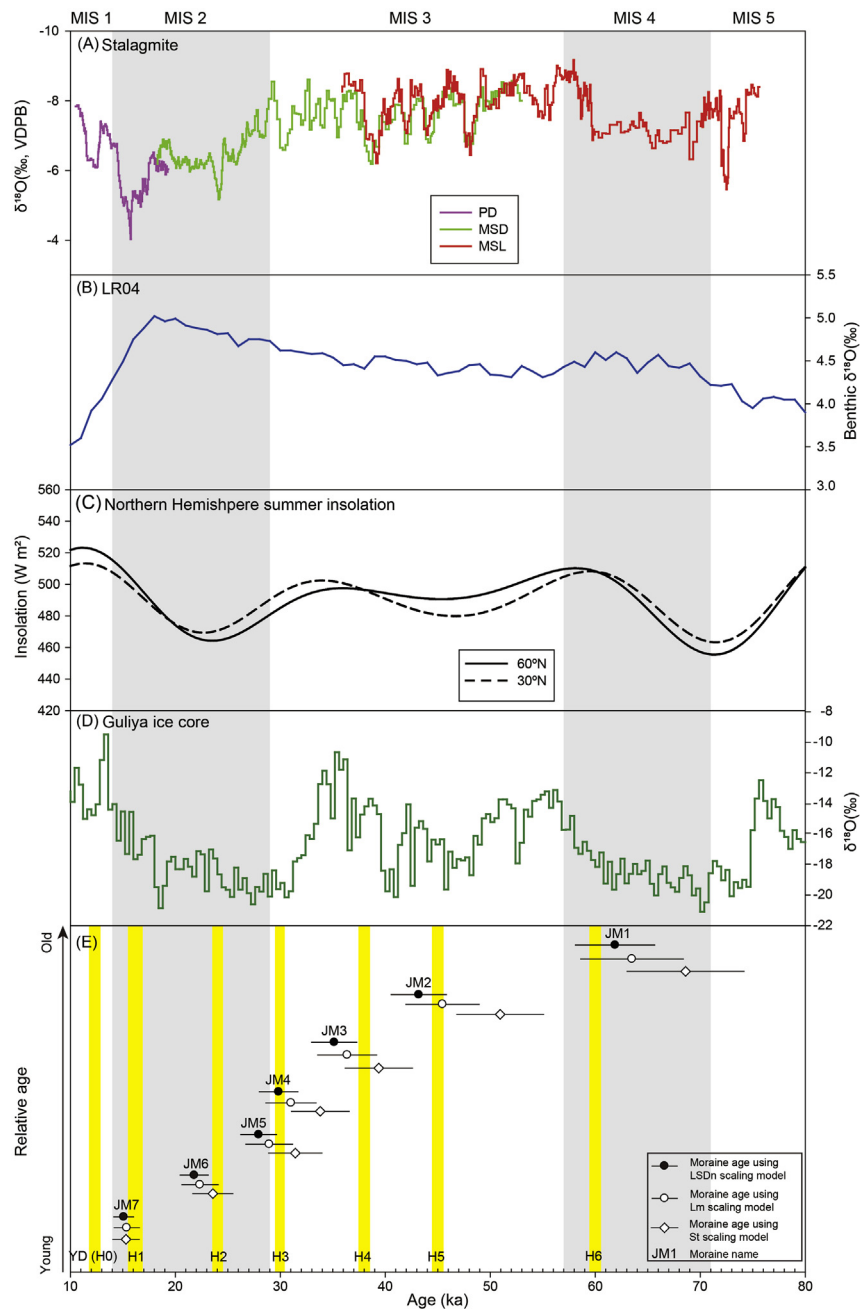
Fig. 5. The last glacial climatic records relative to glacial chronologies constrained by [10]Be surface exposure dating east of Mount Jaggang. (A) The stalagmite δ^{18}O record from Hulu Cave in eastern China (Wang et al., 2001). PD, MSD, and MSL represent different stalagmites sampled from the Hulu Cave. (B) LR04 benthic foraminiferal δ^{18}O stack (Lisiecki and Raymo, 2005), which indicates a combined signature of global temperature and ice volume. (C) Northern Hemisphere summer insolation intensity at 60°N and 30°N (Berger and Loutre, 1991). (D) δ^{18}O records from the Guliya ice core, West Kunlun (Thompson et al., 1997). (E) Plot of the oldest age from different scaling models after rejecting the potential outliers for each moraine east of Mount Jaggang. The YD and Heinrich events are depicted using yellow vertical bands (Bond et al., 1993). (For interpretation of the references to colour in this figure legend, the reader is referred to the Web version of this article.)

North Atlantic climate oscillations, we acknowledge that these are tentatively determined because accurate determination of moraine initial ages relies, in large part, on how well we can estimate the cosmogenic [10]Be production rates whereas there is no direct calibration of production rates across the TP. In addition, although it has been argued that the LSDn scaling model applies well to the high-altitude and low-latitude areas (Lifton et al., 2014), we recognize that there is still lack of complete knowledge of the appropriate scaling model and that moraine initial ages vary with the choice of scaling models.

Exposure-ages are observed to vary between scaling models in the range of 0.4–18.0% (Table 2). The age difference is found below 5% for ages younger than ~17 ka. This value is small relative to that caused by measurements and production rates. However, for ages over ~17 ka, the Lal/Stone time-independent scaling model produces age values ~8.1–18.0% higher over the LSDn scaling model. If these exposure-ages were used to determine moraine initial ages, some moraines (e.g. moraine JM1, JM2, and JM4) would exhibit no correlations with the North Atlantic climate changes (Fig. 5E). Note that the Lal/Stone time-independent model is based on an

assumption of constant [10]Be production rates. Actually, however, [10]Be production rates change over time due to secular changes in the Earth's geomagnetic field (e.g. Lifton, 2016 and references therein). The two scaling models with paleomagnetic corrections (Lm and LSDn in Table 2) yield indistinguishable exposure-ages within 1σ uncertainty for individual sample, supporting the potential teleconnections between the North Atlantic climate oscillations and glacial fluctuations east of Mount Jaggang (Fig. 5E).

6. Conclusion

Cosmogenic [10]Be surface exposure dating was conducted to constrain the glacial chronology east of Mount Jaggang, the Xainza range, central Tibet. The timing of seven moraines was tentatively constrained to ~61.9 ± 3.8 ka, ~43.2 ± 2.6 ka, ~35.1 ± 2.1 ka, ~29.8 ± 1.8 ka, ~27.9 ± 1.7 ka, ~21.8 ± 1.3 ka, and ~15.1 ± 0.9 ka, demonstrating that seven glacial events occurred in the Mount Jaggang area during MIS 4, 3, and 2. The local LGM occurred during MIS 4, and subsequent events became progressively restricted in glacier extent. This pattern of glacial fluctuations might have been caused by decreasing precipitation, which resulted from the reducing intensity of the Asian Summer Monsoon after the MIS 4/3 transition. In addition, these glacial events broadly correspond to the North Atlantic cooling events (Heinrich events), emphasizing the role of temperature as the primary factor affecting glacial activity in the Mount Jaggang area. However, we acknowledge that these correlations remain tentative because of no calibration of [10]Be production rates across the TP.

Acknowledgements

Appendix A. Supplementary data

Supplementary data related to this article can be found at https://doi.org/10.1016/j.quascirev.2018.03.007.

References

Abramowski, U., Bergau, A., Seebach, D., Zech, R., Glaser, B., Sosin, P., Kubik, P.W., Zech, W., 2006. Pleistocene glaciations of Central Asia: results from [10]Be surface exposure ages of erratic boulders from the Pamir (Tajikistan) and the Alay-Turkestan range (Kyrgyzstan). Quat. Sci. Rev. 25, 1080–1096.

Amidon, W.H., Bookhagen, B., Avouac, J., Smith, T., Rood, D., 2013. Late Pleistocene glacial advances in the western Tibet interior. Earth Planet Sci. Lett. 381, 210–221.

An, Z., Colman, S.M., Zhou, W., Li, X., Brown, E.T., Jull, A.J.T., Cai, Y., Huang, Y., Lu, X., Chang, H., Song, Y., Sun, Y., Xu, H., Liu, W., Jin, Z., Liu, X., Cheng, P., Liu, Y., Ai, L., Li, X., Liu, X., Yan, L., Shi, Z., Wang, X., Wu, F., Qiang, X., Dong, J., Lu, F., Xu, X., 2012. Interplay between the westerlies and asian monsoon recorded in lake qinghai sediments since 32 ka. Sci. Rep. 2, 619. https://doi.org/10.1038/Srep00619.

Balco, G., 2011. Contributions and unrealized potential contributions of cosmogenic-nuclide exposure dating to glacier chronology, 1990-2010. Quat. Sci. Rev. 30, 3–27.

Balco, G., Stone, J.O., Lifton, N.A., Dunai, T.J., 2008. A complete and easily accessible means of calculating surface exposure ages or erosion rates from [10]Be and [26]Al measurements. Quat. Geochronol. 3, 174–195.

Benn, D.I., Evans, D.J.A., 2010. Glaciers and Glaciations, second ed. Arnold, London.

Benn, D.I., Owen, L.A., 1998. The role of the Indian summer monsoon and the mid-latitude westerlies in Himalayan glaciation: review and speculative discussion. J. Geol. Soc. 155, 353–363.

Berger, A., Loutre, M.F., 1991. Insolation values for the climate of the last 10 million years. Quat. Sci. Rev. 10, 297–317.

Blomdin, R., Stroeven, A.P., Harbor, J.M., Lifton, N.A., Heyman, J., Gribenski, N., Petrakov, D.A., Caffee, M.W., Ivanov, M.N., Hättestrand, C., Rogozhina, I., Usubaliev, R., 2016. Evaluating the timing of former glacier expansions in the Tian Shan: a key step towards robust spatial correlations. Quat. Sci. Rev. 153, 78–96.

Bond, G., Broecker, W., Johnsen, S., McManus, J., Labeyrie, L., Jouzel, J., Bonani, G., 1993. Correlations between climate records from North Atlantic sediments and Greenland ice. Nature 365, 143–147.

Bookhagen, B., Burbank, D.W., 2006. Topography, relief, and TRMM-derived rainfall variations along the Himalaya. Geophys. Res. Lett. 33, L08405. https://doi.org/10.1029/2006GL026037.

Borchers, B., Marrero, S., Balco, G., Caffee, M., Goehring, B., Lifton, N., Nishiizumi, K., Phillips, F., Schaefer, J., Stone, J., 2016. Geological calibration of spallation production rates in the CRONUS-Earth project. Quat. Geochronol. 31, 188–198.

Briner, J.P., Kaufman, D.S., Manley, W.F., Finkel, R.C., Caffee, M.W., 2005. Cosmogenic exposure dating of late Pleistocene moraine stabilization in Alaska. GSA Bull. 117, 1108–1120.

Chen, Y., Li, Y., Wang, Y., Zhang, M., Cui, Z., Yi, C., Liu, G., 2015. Late Quaternary glacial history of the Karlik Range, easternmost Tian Shan, derived from [10]Be surface exposure and optically stimulated luminescence datings. Quat. Sci. Rev. 115, 17–27.

Chevalier, M., Hilley, G., Tapponnier, P., Van Der Woerd, J., Liu-Zeng, J., Finkel, R.C., Ryerson, F.J., Li, H., Liu, X., 2011. Constraints on the late Quaternary glaciations in Tibet from cosmogenic exposure ages of moraine surfaces. Quat. Sci. Rev. 30, 528–554.

Çiner, A., Sarıkaya, M.A., Yıldırım, C., 2015. Late Pleistocene piedmont glaciations in the Eastern Mediterranean; insights from cosmogenic [36]Cl dating of hummocky moraines in southern Turkey. Quat. Sci. Rev. 116, 44–56.

Clark, P.U., Dyke, A.S., Shakun, J.D., Carlson, A.E., Clark, J., Wohlfarth, B., Mitrovica, J.X., Hostetler, S.W., McCabe, A.M., 2009. The last glacial maximum. Science 325, 710–714.

Crump, S.E., Anderson, L.S., Miller, G.H., Anderson, R.S., 2017. Interpreting exposure ages from ice-cored moraines: a Neoglacial case study on Baffin Island, Arctic Canada. J. Quat. Sci. 32, 1049–1062.

Desilets, D., Zreda, M., 2003. Spatial and temporal distribution of secondary cosmic-ray nucleon intensities and applications to in-situ cosmogenic dating. Earth Planet Sci. Lett. 206, 21–42.

Desilets, D., Zreda, M., Prabu, T., 2006. Extended scaling factors for in situ cosmogenic nuclides: new measurements at low latitude. Earth Planet Sci. Lett. 246, 265–276.

Dong, G., Xu, X., Zhou, W., Fu, Y., Zhang, L., Li, M., 2017a. Cosmogenic [10]Be surface exposure dating and glacier reconstruction for the last glacial maximum in the quemuqu valley, western Nyainqentanglha mountains, south Tibet. J. Quat. Sci. 32, 639–652.

Dong, G., Yi, C., Chen, L., 2010. An introduction to the physical geography of the Qiangtang Plateau: a frontier for future geoscience research on the Tibetan Plateau. Phys. Geogr. 31, 475–492.

Dong, G., Yi, C., Caffee, M.W., 2014. [10]Be dating of boulders on moraines from the last glacial period in the Nyainqentanglha mountains. Tibet. Sci. China. Earth. Sci. 57, 221–231.

Dong, G., Zhou, W., Yi, C., Zhang, L., Li, M., Fu, Y., Zhang, Q., 2017b. Cosmogenic [10]Be surface exposure dating of 'Little Ice Age' glacial events in the Mount Jaggang area, central Tibet. Holocene 27, 1516–1525.

Dortch, J.M., Owen, L.A., Caffee, M.W., 2013. Timing and climatic drivers for glaciation across semi-arid western Himalayan-Tibetan orogen. Quat. Sci. Rev. 78, 188–208.

Dortch, J.M., Owen, L.A., Haneberg, W.C., Caffee, M.W., Dietsch, C., Kamp, U., 2009. Nature and timing of large landslides in the Himalaya and Transhimalaya of northern India. Quat. Sci. Rev. 28, 1037–1054.

Dunai, T., 2001. Influence of secular variation of the geomagnetic field on production rates of in situ produced cosmogenic nuclides. Earth Planet Sci. Lett. 193, 197–212.

Finkel, R.C., Owen, L.A., Barnard, P.L., Caffee, M.W., 2003. Beryllium-10 dating of Mount Everest moraines indicates a strong monsoon influence and glacial synchroneity throughout the Himalaya. Geology 31, 561–564.

Fu, P., Stroeven, A.P., Harbor, J.M., Hättestrand, C., Heyman, J., Caffee, M.W., Zhou, L., 2013. Paleoglaciation of shaluli Shan, southeastern Tibetan plateau. Quat. Sci. Rev. 64, 121–135.

Gillespie, A., Molnar, P., 1995. Asynchronous maximum advances of mountain and continental glaciers. Rev. Geophys. 33, 311–364.

Gosse, J.C., Phillips, F.M., 2001. Terrestrial in situ cosmogenic nuclides: theory and application. Quat. Sci. Rev. 20, 1475–1560.

Hallet, B., Putkonen, J., 1994. Surface dating of dynamic landforms: young boulders on aging moraines. Science 265, 937–940.

Han, Y., Fang, X., Kang, S., Wang, H., Kang, F., 2008. Shifts of dust source regions over central Asia and the Tibetan Plateau: connections with the Arctic oscillation and the westerly jet. Atmos. Environ. 10, 2358–2368.

He, Y., Bao, Z., Hou, J., Brown, E.T., Wang, M., Xie, S., Yi, C., 2016. Variation of the mid-latitude westerlies and Indian summer monsoon since the last deglaciation: evidence from grain-size data from Linggo Co, central Tibet. Chin. Sci. Bull. 61, 3583–3595 (In Chinese).

Heinrich, H., 1988. Origin and consequences of cyclic ice rafting in the Northeast Atlantic Ocean during the past 130,000 years. Quat. Res. 29, 142–152.

Hemming, S.R., 2004. Heinrich events: massive late Pleistocene detritus layers of the North Atlantic and their global climate imprint. Rev. Geophys. 42, RG1005. https://doi.org/10.1029/2003RG000128.

Herzschuh, U., 2006. Palaeo-moisture evolution in monsoonal Central Asia during the last 50,000 years. Quat. Sci. Rev. 25, 163–178.

Heyman, J., 2014. Paleoglaciation of the Tibetan Plateau and surrounding mountains based on exposure ages and ELA depression estimates. Quat. Sci. Rev. 91, 30–41.

Heyman, J., Applegate, P.J., Blomdin, R., Gribenski, N., Harbor, J.M., Stroeven, A.P., 2016. Boulder height - exposure age relationships from a global glacial [10]Be compilation. Quat. Geochronol. 34, 1–11.

Heyman, J., Stroeven, A.P., Caffee, M.W., Hättestrand, C., Harbor, J.M., Li, Y., Alexanderson, H., Zhou, L., Hubbard, A., 2011a. Palaeoglaciology of Bayan Har Shan, NE Tibetan Plateau: exposure ages reveal a missing LGM expansion. Quat. Sci. Rev. 30, 1988–2001.

Heyman, J., Stroeven, A.P., Harbor, J.M., Caffee, M.W., 2011b. Too young or too old: evaluating cosmogenic exposure dating based on an analysis of compiled boulder exposure ages. Earth Planet Sci. Lett. 302, 71–80.

Hong, Y., Hong, B., Lin, Q., Zhu, Y., Shibata, Y., Hirota, M., Uchida, M., Leng, X., Jiang, H., Xu, H., Wang, H., Yi, L., 2003. Correlation between indian ocean summer monsoon and North atlantic climate during the holocene. Earth Planet Sci. Lett. 211, 371–380.

Hu, G., Yi, C., Zhang, J., Dong, G., Liu, J., Xu, X., Jiang, T., 2016. Extensive glacial advances during the Last Glacial Maximum near the eastern Himalayan syntaxis. Quat. Int. 443, 1–12.

Hughes, P.D., Gibbard, P.L., Ehlers, J., 2013. Timing of glaciation during the last glacial cycle: evaluating the concept of a global 'Last Glacial Maximum' (LGM). Earth Sci. Rev. 125, 171–198.

Kasper, T., Haberzettl, T., Wang, J., Daut, G., Doberschütz, S., Zhu, L., Mäusbacher, R., 2015. Hydrological variations on the Central Tibetan Plateau since the Last Glacial Maximum and their teleconnection to inter-regional and hemispheric climate variations. J. Quat. Sci. 30, 70–78.

Kohl, C.P., Nishiizumi, K., 1992. Chemical isolation of quartz for measurement of in-situ-produced cosmogenic nuclides. Geochim. Cosmochim. Acta 56, 3583–3587.

Koppes, M., Gillespie, A.R., Burke, R.M., Thompson, S.C., Stone, J., 2008. Late quaternary glaciation in the kyrgyz tien shan. Quat. Sci. Rev. 27, 846–866.

Lal, D., 1991. Cosmic ray labeling of erosion surfaces: in situ nuclide production rates and erosion models. Earth Planet Sci. Lett. 104, 424–439.

Lehmkuhl, F., Klinge, M., Rother, H., Hülle, D., 2016. Distribution and timing of Holocene and late Pleistocene glacier fluctuations in western Mongolia. Ann. Glaciol. 57, 169–178.

Li, X., Liang, J., Hou, J., Zhang, W., 2015. Centennial-scale climate variability during the past 2000 years on the central Tibetan Plateau. Holocene 25, 892–899.

Li, Y., 2013. Determining topographic shielding from digital elevation models for cosmogenic nuclide analysis: a GIS approach and field validation. J. Mt. Sci. 10, 355–362.

Li, Y., Liu, G., Chen, Y., Li, Y., Harbor, J., Stroeven, A.P., Caffee, M., Zhang, M., Li, C., Cui, Z., 2014. Timing and extent of Quaternary glaciations in the Tianger Range, eastern Tian Shan, China, investigated using [10]Be surface exposure dating. Quat. Sci. Rev. 98, 7–23.

Lisiecki, L.E., Raymo, M.E., 2005. A Pliocene-Pleistocene stack of 57 globally distributed benthic δ^{18}O records. Paleoceanography 20, PA1003. https://doi.org/10.1029/2004PA001071.

Lifton, N., 2016. Implications of two Holocene time-dependent geomagnetic models for cosmogenic nuclide production rate scaling. Earth Planet Sci. Lett. 433, 257–268.

Lifton, N., Bieber, J.W., Clem, J.M., Duldig, M.L., Evenson, P., Humble, J.E., Pyle, R., 2005. Addressing solar modulation and long-term uncertainties in scaling secondary cosmic rays for in situ cosmogenic nuclide applications. Earth Planet Sci. Lett. 239, 140–161.

Lifton, N., Sato, T., Dunai, T.J., 2014. Scaling in situ cosmogenic nuclide production rates using analytical approximations to atmospheric cosmic-ray fluxes. Earth Planet Sci. Lett. 386, 149–160.

Mix, A.C., Bard, E., Schneider, R., 2001. Environmental processes of the ice age: land, oceans, glaciers (EPILOG). Quat. Sci. Rev. 20, 627–657.

Nishiizumi, K., Imamura, M., Caffee, M.W., Southon, J.R., Finkel, R.C., McAninch, J., 2007. Absolute calibration of [10]Be AMS standards. Nucl. Instrum. Methods Phys. Res. Sect. B Beam Interact. Mater. Atoms 258, 403–413.

Oerlemans, J., 2005. Extracting a climate signal from 169 glacier records. Science 308, 675–677.

Owen, L.A., Chen, J., Hedrick, K.A., Caffee, M.W., Robinson, A.C., Schoenbohm, L.M., Yuan, Z., Li, W., Imrecke, D.B., Liu, J., 2012. Quaternary glaciation of the tashkurgan valley, southeast Pamir. Quat. Sci. Rev. 47, 56–72.

Owen, L.A., Dortch, J.M., 2014. Nature and timing of Quaternary glaciation in the Himalayan-Tibetan orogen. Quat. Sci. Rev. 88, 14–54.

Owen, L.A., Finkel, R.C., Caffee, M.W., 2002a. A note on the extent of glaciation throughout the Himalaya during the global Last Glacial Maximum. Quat. Sci. Rev. 21, 147–157.

Owen, L.A., Finkel, R.C., Caffee, M.W., Gualtieri, L., 2002b. Timing of multiple late Quaternary glaciations in the Hunza Valley, Karakoram Mountains, northern Pakistan: defined by cosmogenic radionuclide dating of moraines. Geol. Soc. Am. Bull. 114, 593–604.

Owen, L.A., Finkel, R.C., Ma, H., Spencer, J.Q., Derbyshire, E., Barnard, P.L., Caffee, M.W., 2003. Timing and style of late quaternary glaciation in northeastern Tibet. Geol. Soc. Am. Bull. 115, 1356–1364.

Owen, L.A., Yi, C., Finkel, R.C., Davis, N.K., 2010. Quaternary glaciation of gurla mandhata (Naimon'anyi). Quat. Sci. Rev. 29, 1817–1830.

Phillips, F.M., Zreda, M.G., Benson, L.V., Plummer, M.A., Elmore, D., Sharma, P., 1996. Chronology for fluctuations in late Pleistocene Sierra Nevada glaciers and lakes. Science 274, 749–751.

Phillips, W.M., Sloan, V.F., Shroder Jr., J.F., Sharma, P., Clarke, M.L., Rendell, H.M., 2000. Asynchronous glaciation at nanga parbat, northwestern Himalaya mountains, Pakistan. Geology 28, 431–434.

Porter, S.C., An, Z.S., 1995. Correlation between climate events in the North Atlantic and China during the last glaciation. Nature 375, 305–308.

Putkonen, J., Swanson, T., 2003. Accuracy of cosmogenic ages for moraines. Quat. Res. 59, 255–261.

Röhringer, I., Zech, R., Abramowski, U., Sosin, P., Aldahan, A., Kubik, P.W., Zöller, L., Zech, W., 2012. The late Pleistocene glaciation in the Bogchigir Valleys (Pamir, Tajikistan) based on [10]Be surface exposure dating. Quat. Res. 78, 590–597.

Rother, H., Stauch, G., Loibl, D., Lehmkuhl, F., Freeman, S.P.H.T., 2017. Late Pleistocene glaciations at Lake Donggi Cona, eastern Kunlun Shan (NE Tibet): early maxima and a diminishing trend of glaciation during the last glacial cycle. Boreas 46, 503–524.

Rupper, S., Roe, G., Gillespie, A., 2009. Spatial patterns of Holocene glacier advance and retreat in Central Asia. Quat. Res. 72, 337–346.

Scherler, D., Bookhagen, B., Strecker, M.R., von Blanckenburg, F., Rood, D., 2010. Timing and extent of late Quaternary glaciation in the western Himalaya constrained by [10]Be moraine dating in Garhwal, India. Quat. Sci. Rev. 29, 815–831.

Seong, Y., Owen, L.A., Yi, C., Finkel, R.C., 2009. Quaternary glaciation of Muztag Ata and Kongur Shan: evidence for glacier response to rapid climate changes throughout the late glacial and holocene in westernmost Tibet. Geol. Soc. Am. Bull. 121, 348–365.

Shi, Y., Yao, T., 2002. MIS3b (54~44 ka BP) cold period and glacial advance in middle and low latitudes. J. Glaciol. Geocryol. 24, 1–9 (in Chinese).

Shi, Y., Yu, G., Liu, X., Li, B., Yao, T., 2001. Reconstruction of the 30-40 ka BP enhanced Indian monsoon climate based on geological records from the Tibetan Plateau. Palaeogeogr. Palaeoclimatol. Palaeoecol. 169, 69–83.

Shi, Y., Zheng, B., Yao, T., 1997. Glaciers and environments during the last glacial maximum (LGM) on the Tibetan plateau. J. Glaciol. Geocryol. 19, 97–113 (In Chinese).

Stone, J.O., 2000. Air pressure and cosmogenic isotope production. J. Geophys. Res. 105, 23753–23759.

Strasky, S., Graf, A.A., Zhao, Z., Kubik, P.W., Baur, H., Schlüchter, C., Wieler, R., 2009. Late Glacial ice advances in southeast Tibet. J. Asian Earth Sci. 34, 458–465.

Thompson, L.G., Yao, T., Davis, M.E., Henderson, K.A., Mosley-Thompson, E., Lin, P.-N., Beer, J., Synal, H.-A., Cole-Dai, J., Bolzan, J.F., 1997. Tropical climate instability: the last glacial cycle from a Qinghai-Tibetan ice core. Science 276, 1821–1825.

Vandenberghe, J., Renssen, H., van Huissteden, K., Nugteren, G., Konert, M., Lu, H., Dodonov, A., Buylaert, J., 2006. Penetration of atlantic westerly winds into central and east asia. Quat. Sci. Rev. 25, 2380–2389.

Voelker, A.H.L., workshop participants, 2002. Global distribution of centennial-scale records for Marine Isotope Stage (MIS) 3: a database. Quat. Sci. Rev. 21, 1185–1212.

Wang, J., 2010. Glacial advance in the Qinghai-Tibet Plateau and peripheral mountains during the mid-MIS 3. Quat. Sci. 30, 1055–1065 (in Chinese).

Wang, J., Kassab, C., Harbor, J.M., Caffee, M.W., Cui, H., Zhang, G., 2013. Cosmogenic nuclide constraints on late Quaternary glacial chronology on the Dalijia Shan, northeastern Tibetan Plateau. Quat. Res. 79, 439–451.

Wang, Y., Cheng, H., Edwards, R.L., An, Z., Wu, J., Shen, C., Dorale, J.A., 2001. A high-resolution absolute-dated late Pleistocene monsoon record from Hulu cave, China. Science 294, 2345–2348.

Xu, X., Dong, G., Pan, B., 2014. Modelling glacier advances and related climate conditions during the last glaciation cycle in the Kuzigun Valley, Tashkurgan catchment, on the north-west Tibetan Plateau. J. Quat. Sci. 29, 279–288.

Xu, X., Hu, G., Qiao, B., 2013. Last glacial maximum climate based on cosmogenic [10]Be exposure ages and glacier modeling for the head of Tashkurgan Valley, northwest Tibetan Plateau. Quat. Sci. Rev. 80, 91–101.

Xu, X., Yi, C., 2014. Little ice age on the Tibetan plateau and its bordering mountains: evidence from moraine chronologies. Glob. Planet. Change 116, 41–53.

Yang, J., Chen, Y., Xu, X., Cui, Z., Xiong, H., 2017. Quaternary glacial history of the Kanas Valley, Chinese Altai, NW China, constrained by electron spin resonance and optically stimulated luminescence datings. J. Asian Earth Sci. 147, 164–177.

Zech, R., 2012. A late Pleistocene glacial chronology from the Kitschi-Kurumdu Valley, Tien Shan (Kyrgyzstan), based on [10]Be surface exposure dating. Quat. Res. 77, 281–288.

Zech, R., Abramowski, U., Glaser, B., Sosin, P., Kubik, P.W., Zech, W., 2005a. Late Quaternary glacial and climate history of the Pamir Mountains derived from cosmogenic [10]Be exposure ages. Quat. Res. 64, 212–220.

Zech, R., Glaser, B., Sosin, P., Kubik, P.W., Zech, W., 2005b. Evidence for long-lasting landform surface instability on hummocky moraines in the Pamir Mountains (Tajikistan) from [10]Be surface exposure dating. Earth Planet Sci. Lett. 237, 453–461.

Zech, R., Röhringer, I., Sosin, P., Kabgov, H., Merchel, S., Akhmadaliev, S., Zech, W., 2013. Late Pleistocene glaciations in the Gissar Range, Tajikistan, based on [10]Be surface exposure dating. Palaeogeogr. Palaeoclimatol. Palaeoecol. 369, 253–261.

Zhang, L., Wu, Z., Chang, H., Li, M., Dong, G., Fu, Y., Zhao, G., Zhou, W., 2016. A case study using [10]Be-[26]Al exposure dating at the Xi'an AMS Center. Radiocarbon 58, 193–203.

Zhao, J., Song, Y., King, J.W., Liu, S., Wang, J., Wu, M., 2010. Glacial geomorphology

and glacial history of the Muzart River valley, Tianshan range, China. Quat. Sci. Rev. 29, 1453–1463.

Zhu, L., Lü, X., Wang, J., Peng, P., Kasper, T., Daut, G., Haberzettl, T., Frenzel, P., Li, Q.,

Yang, R., Schwalb, A., Mäusbacher, R., 2015. Climate change on the Tibetan Plateau in response to shifting atmospheric circulation since the LGM. Sci. Rep. 5, 13318. https://doi.org/10.1038/srep13318.